

The spatial and velocity bias of linear density peaks and protohaloes in the Λ cold dark matter cosmology

Anna Elia^{*}, Aaron D. Ludlow and Cristiano Porciani

Argelander Institut für Astronomie der Universität Bonn, Auf dem Hügel 71, D-53121 Bonn, Germany

5 November 2018

ABSTRACT

We use high resolution N-body simulations to investigate the Lagrangian bias of cold dark matter haloes within the Λ cold dark matter cosmology. Our analysis focuses on ‘protohaloes’, which we identify in the simulation initial conditions with the subsets of particles belonging to individual redshift-zero haloes. We then calculate the number-density and velocity-divergence fields of protohaloes and estimate their auto spectral densities. We also measure the corresponding cross spectral densities with the linear matter distribution. We use our results to test a Lagrangian-bias model presented by Desjacques and Sheth which is based on the assumption that haloes form out of local density maxima of a specific height. Our comparison validates the predicted functional form for the scale-dependence of the bias for both the density and velocity fields. We also show that the bias coefficients are accurately predicted for the velocity divergence. On the contrary, the theoretical values for the density bias parameters do not accurately match the numerical results as a function of halo mass. This is likely due to the simplistic assumptions that relate virialized haloes to density peaks of a given height in the model. We also detect appreciable stochasticity for the Lagrangian density bias, even on very large scales. These are not included in the model at leading order but correspond to higher order corrections.

Key words: methods:analytical – numerical – galaxies: haloes – cosmology: theory – large-scale structure of Universe.

1 INTRODUCTION

Galaxy redshift surveys are powerful probes of cosmology. The main observables able to constrain cosmological parameters are the overall shape of the galaxy power spectrum at wavenumbers $k < 0.1 \text{ Mpc}^{-1}$ and the baryonic acoustic oscillations within it. These are treated as proxies for the matter power spectrum for which we can make robust theoretical predictions. Galaxies, however, are biased tracers of the cosmic mass distribution and many features appearing in their power spectrum depend on how a specific observational sample was selected. To reconstruct the matter power spectrum we thus need an accurate bias model whose free coefficients should be used as nuisance parameters and marginalized over. In the era of precision cosmology, where measurements of the matter power spectrum with per cent accuracy are required, this task is particularly demanding.

Bias models can be divided into two broad classes. Eulerian biasing schemes relate the galaxy density contrast, $\delta_g(\mathbf{x}, t)$, to the matter density distribution, δ , evaluated at the same time t (but not necessarily at the same spa-

tial location). After smoothing the fields on large scales, so that $|\delta|$ is typically much smaller than unity, one can write (Fry & Gaztañaga 1993)

$$\begin{aligned} \delta_g(\mathbf{x}) = & B_0 + \int d^3x_1 B_1(\mathbf{x} - \mathbf{x}_1) \delta(\mathbf{x}_1) + \\ & + \frac{1}{2} \int d^3x_1 d^3x_2 B_2(\mathbf{x} - \mathbf{x}_1, \mathbf{x} - \mathbf{x}_2) \delta(\mathbf{x}_1) \delta(\mathbf{x}_2) + \\ & + \dots, \end{aligned} \quad (1)$$

where all fields are evaluated at the same time t and the details of the bias model are specified by the kernel functions, B_i . If one further assumes that biasing is local (i.e. that all kernels can be written as products of Dirac delta distributions), this reduces to

$$\delta_g(\mathbf{x}) = b_0 + b_1 \delta(\mathbf{x}) + \frac{b_2}{2} \delta^2(\mathbf{x}) + \dots, \quad (2)$$

where now the bias coefficients b_i are real numbers.

In Lagrangian bias models, on the other hand, one considers the regions in the initial conditions that will collapse to form galaxies (or their hosting dark-matter haloes) at time t and writes their density contrast, $\delta_g^L(\mathbf{q})$, in terms of the linear density contrast, $\delta_0(\mathbf{q})$. Large-scale expansions

^{*} E-mail: elia@astro.uni-bonn.de

analogous to eqs. (1) and (2) can also be written in this case. As a second step, one must determine the final position, $\mathbf{x}(\mathbf{q}, t)$, of a fluid element initially located at \mathbf{q} , and compute $\delta_g(\mathbf{x}(\mathbf{q}, t), t)$ out of $\delta_g^L(\mathbf{q})$. This Lagrangian-to-Eulerian mapping (LEM) accounts for gravitationally induced motions that determine the final position of the objects.

Local Eulerian and Lagrangian bias schemes are not equivalent; they generate a different shape for the galaxy bispectrum (Catelan et al. 2000) and are not compatible within the framework of perturbation theory (Matsubara 2011). In fact, Catelan et al. (1998) have shown that a local Lagrangian biasing scheme generates a non-linear, non-local and stochastic bias in Eulerian space. On the other hand, non-local Eulerian and Lagrangian schemes are equivalent and can be seen as different mathematical representations of the same physical process (Matsubara 2011).

Due to its simplicity, the local Eulerian model is by far the most widely used in practical applications, such as perturbative calculations. However, it is purely phenomenological and does not have a strong theoretical motivation. Detailed comparison with numerical simulations has also evidenced its limited validity (e.g. Roth & Porciani 2011, Pollack, Smith & Porciani 2011). Physical models of bias are generally given in the Lagrangian framework as conditions on galaxy (halo) formation are more easily imposed onto the linear density field using some model for the collapse of density perturbations. Mo & White (1996, hereafter MW) used a Press-Schechter-like argument (Press & Schechter 1974) to compute the bias coefficients of a local Lagrangian scheme as a function of halo mass. The same authors also showed how these parameters can be combined to calculate the bias coefficients of a local Eulerian scheme assuming that large-scale density perturbations follow the spherical collapse model. The effect of non-linear shear on the LEM was discussed by Catelan et al. (1998) using the Zel'dovich approximation (Zel'dovich 1970). For halo masses $M > M_*(z)$ (where $M_*(z)$ is the characteristic mass for collapse at redshift z) the MW formula for b_1 is in good agreement with the predictions of N-body simulations (Mo, Jing & White 1997). At lower masses, however, the agreement rapidly deteriorates (Jing 1998). Porciani, Catelan & Lacey (1999) and Jing (1999) showed that the discrepancy between the N-body simulations and the analytical predictions is already present in Lagrangian space and should thus be attributed to the limitations of the Press-Schechter formalism rather than to the approximated treatment of the LEM.

The Lagrangian bias emerging from the extended Press-Schechter model (Bond et al. 1991) was first derived by Porciani et al. (1998), rediscussed in Scannapieco & Barkana (2002) and tested against simulations by Scannapieco & Thacker (2005). This approach follows correlated trajectories of δ_0 at different Lagrangian locations as a function of the smoothing scale and looks for correlations in the first-crossing scales of a density threshold.

According to the peak-background-split argument (Bardeen et al. 1986; Cole & Kaiser 1989), long-wavelength density fluctuations modulate halo formation by modifying the collapse time of localized short-wavelength perturbations. This makes it possible to generalise the calculation of the Lagrangian MW bias coefficients to any model for

the halo mass function (Sheth & Tormen 1999, Tinker et al. 2010, Giannantonio & Porciani 2010) and to improve the agreement with N-body simulations (Seljak & Warren 2004, Tinker et al. 2005, Gao et al. 2005, Pillepich et al. 2010).

Kaiser (1984) explained the strong clustering of Abell clusters by assuming that they originate from the regions above a density threshold in the (suitably smoothed) linear density field. Following this line of reasoning, it is common to assume that dark-matter haloes form out of linear density peaks, as an alternative to the Press-Schechter approach. Tests against N-body simulations have shown that this is a well justified assumption, especially for massive haloes (Ludlow & Porciani 2011, see also Frenk et al. 1988). The statistical properties of the local maxima in a Gaussian random field have been extensively studied by Bardeen et al. (1986) (see also Peacock & Heavens 1985 and Hoffman & Shaham 1985). Mo, Jing & White (1997) introduced peaks theory in the MW formalism, while Matsubara (1999) evaluated the level of stochasticity in the Lagrangian clustering of density extrema.

Recently, Desjacques (2008) and Desjacques & Sheth (2010, hereafter DS) showed that the correlation of density peaks in real and redshift space can be interpreted in terms of a simple Lagrangian biasing scheme. Due to the peak constraint, the effective Lagrangian peak density at a given point not only depends on the local value of the mass density but also on its Laplacian. The first-order peak bias depends on the mass and height of the peaks, and on the matter power spectrum. For high peaks, this reduces to the results by Matsubara (1999). Moreover, although peaks move with the matter at their positions, DS infer the existence of a statistical velocity bias due to the fact that local maxima can only exist at special locations. This also leads to a bias between the linear velocity spectra of peaks and matter which is predictable in quantitative terms.

In spite of the fact that the DS model provides the initial conditions for sophisticated models of the (Eulerian) halo distribution where the LEM is based either on resummed perturbation theory (Elia et al. 2011) or on the Zel'dovich approximation (Desjacques et al. 2010), its predictions for the Lagrangian clustering and velocities of the regions that will form collapsed structures have never been thoroughly tested against numerical simulations. This paper provides such a test, which is necessary if we are to use advanced bias models to extract useful information on the cosmological parameters through a comparison with observations.

The structure of the paper is as follows. In Section 2 we review the bias model first presented in DS. The details of our N-body simulations and analysis techniques are outlined in Section 3, and a comparison between the model and numerical results is presented in Section 4. Finally, we summarize our main results in Section 5.

2 THE DS MODEL

In this section we summarize, for completeness, the peaks model described in Section 2 of DS. In order to do so, we first introduce and define some quantities relevant for peak statistics.

The spectral moments of the matter power spectrum are defined as

$$\sigma_n^2(R_s, z) = \frac{1}{2\pi^2} \int_0^\infty dk k^{2(n+1)} P(k, z) W(k, R_s)^2, \quad (3)$$

where $P(k, z)$ is the linear matter power spectrum at redshift z , and $W(k, R_s)$ is a smoothing kernel of characteristic length R_s . In terms of the moments we define the spectral parameters:

$$\gamma_n \equiv \frac{\sigma_n^2}{\sigma_{n-1}\sigma_{n+1}}. \quad (4)$$

There are two common choices for $W(k, R_s)$: the Gaussian filter

$$W_G(k, R_s) = e^{-\frac{k^2 R_s^2}{2}}, \quad (5)$$

and the top-hat filter

$$W_{TH}(k, R_s) = \frac{3[\sin(kR_s) - kR_s \cos(kR_s)]}{k^3 R_s^3}. \quad (6)$$

The mass contained within the comoving length R_s in these cases is

$$M_G(R_s) = (2\pi)^{3/2} \bar{\rho} R_s^3, \text{ and } M_{TH}(R_s) = \frac{4\pi}{3} \bar{\rho} R_s^3, \quad (7)$$

where $\bar{\rho}$ is the mean matter density of the Universe.

We will often characterize peaks in terms of their dimensionless peak height, ν , defined

$$\nu(R_s, z_c) = \frac{\delta_p}{\sigma_0(R_s, z_c)}. \quad (8)$$

Here δ_p is the smoothed overdensity at the peak location linearly extrapolated to $z = 0$, and $\sigma_0(R_s, z_c)$ is the linear rms mass fluctuation in spheres of radius R_s . DS linked density maxima of height $\nu(R_s, z)$ to dark matter haloes of mass M_s collapsing at redshift z_c , assuming that δ_p coincides with the threshold for collapse, δ_c .

Bardeen et al. (1986) and DS computed the cross-correlation between peaks and the underlying density field which also corresponds to the average density profile around density maxima. Similarly, Desjacques (2008) evaluated the leading order expressions (on large spatial separations) for the peak auto-correlation function and the line-of-sight mean streaming for pairs of discrete local maxima of height ν . Desjacques (2008) and DS showed that the full expression for the cross-correlation and the large-scale asymptotic of the auto-correlation function are consistent with – and thus can be thought of as arising from – an effective bias relation. In the DS model, the number density and the velocity of peaks, δn_{pk} and \mathbf{v}_{pk} , are related to the dark matter density contrast and velocity fields, linearly extrapolated to $z = 0$, via:

$$\delta n_{pk}(\mathbf{x}|z_c) = b_\nu \delta_S(\mathbf{x}) - b_\zeta \nabla^2 \delta_S(\mathbf{x}), \quad (9)$$

and

$$\mathbf{v}_{pk}(\mathbf{x}|z_c) = \mathbf{v}_S(\mathbf{x}) - \frac{\sigma_0^2}{\sigma_1^2} \nabla \delta_S(\mathbf{x}). \quad (10)$$

The subscript ‘‘S’’ indicates that the fields are smoothed on the scale R_s , and the bias parameters, b_ν and b_ζ , are given by

$$b_\nu = \frac{1}{\sigma_0} \left(\frac{\nu - \gamma_1 \bar{u}}{1 - \gamma_1^2} \right), \quad (11)$$

and

$$b_\zeta = \frac{1}{\sigma_2} \left(\frac{\bar{u} - \gamma_1 \nu}{1 - \gamma_1^2} \right). \quad (12)$$

Here \bar{u} is the mean curvature of the peaks, which can be approximated by (Bardeen et al. 1986)

$$\bar{u} = \gamma_1 \nu + \frac{3(1 - \gamma_1^2) + (1.216 - 0.9\gamma_1^4) \exp\left[-\frac{\gamma_1}{2} \left(\frac{\gamma_1 \nu}{2}\right)^2\right]}{\left[3(1 - \gamma_1^2) + 0.45 + \left(\frac{\gamma_1 \nu}{2}\right)^2\right]^{\frac{1}{2}} + \left(\frac{\gamma_1 \nu}{2}\right)}. \quad (13)$$

Note that b_ν coincides with the peak bias factor found by Bardeen et al. (1986) after neglecting the derivatives of the density correlation function.

Since, by definition, the gradient of the density field vanishes at peak locations, eq. (10) suggests that the peak and dark matter velocity fields must be coincident there. By construction, *peaks move with the dark matter flow*, yet the spatial bias induces a statistical velocity bias. We will consider the scaled velocity divergence, $\theta(\mathbf{x}) = \nabla \times \mathbf{v}(\mathbf{x}) / (aHf)$, rather than the velocity field. Here a is the scale factor, H the Hubble parameter, $f = d \ln D / d \ln a$, with D the linear growth factor. In these units, both $\theta(\mathbf{x})$ and $\delta(\mathbf{x})$ are dimensionless quantities. With these changes, eqs. (9) and (10) can be rewritten in Fourier space as

$$\delta n_{pk}(\mathbf{k}) = (b_\nu + b_\zeta k^2) \delta(\mathbf{k}) W(k, R_s) \quad (14)$$

and

$$\theta_{pk}(\mathbf{k}) = (1 - b_\sigma k^2) \theta(\mathbf{k}) W(k, R_s) = b_{vel}(k) \theta(\mathbf{k}), \quad (15)$$

where we have defined

$$b_\sigma = \frac{\sigma_0^2}{\sigma_1^2}. \quad (16)$$

In the limit of high peaks ($\nu \gg 1$) it can be shown that the bias parameters obey the following asymptotic relations: $b_\nu \rightarrow \nu/\sigma_0$ and $b_\zeta \rightarrow 0$. This implies that the highest peaks are linearly biased tracers of the underlying matter field. This is consistent with the predictions of the peak-background split (Mo, Jing & White 1997) and DS showed that, indeed, b_ν is the appropriate generalization of the constant, large-scale bias for low ν . Unlike the density bias factors, b_σ does not depend on ν .

In order to test this model against N-body simulations, we will make use of the cross-spectra between the peak and dark matter densities and velocities (denoted as P_{mp} and \mathcal{P}_{mp} , respectively) and of the corresponding peak auto-spectra (P_p and \mathcal{P}_p). From eqs. (14) and (15) we obtain

$$\begin{aligned} P_{mp}(k) &= (b_\nu + b_\zeta k^2) P(k) W(k, R_s), \\ P_p(k) &\simeq (b_\nu + b_\zeta k^2)^2 P(k) W^2(k, R_s), \end{aligned} \quad (17)$$

$$\begin{aligned} \mathcal{P}_{mp}(k) &\simeq (1 - b_\sigma k^2) \mathcal{P}(k) W(k, R_s), \\ \mathcal{P}_p(k) &\simeq (1 - b_\sigma k^2)^2 \mathcal{P}(k) W^2(k, R_s), \end{aligned} \quad (18)$$

where $P(k)$ and $\mathcal{P}(k)$ are the matter density and velocity divergence auto-spectra, respectively. We remind the reader that the expression for $P_p(k)$ is only valid to first order in $P(k)$ as $k \rightarrow 0$, and that higher order corrections should be included to improve its accuracy (see e.g. Desjacques et al. 2010). On the contrary, the expression for the cross-spectrum P_{mp} is exact, as shown in Bardeen et al.

(1986) and in the Appendix A of DS. Eq. (17) has the same functional form as eq. (57) in Matsubara (1999) who studied the clustering of density extrema. The DS coefficients b_ν and b_ζ match those in Matsubara (1999) only in the limit $\nu \gg 1$, for which nearly all extrema are density maxima.

3 NUMERICAL ISSUES

In this section we provide a brief description of the main numerical issues relevant for this work. This includes a brief description of our numerical simulations in Section 3.1, our main analysis techniques in Section 3.2, and a characterization of halo collapse barriers in Section 3.3.

3.1 N-body simulations

Our analysis focuses on two high-resolution N-body simulations of structure formation in the standard LCDM cosmology. The cosmological parameters for our runs were chosen to be consistent with the fifth-year WMAP data release (Komatsu et al. 2009). These are $h = 0.701$, $\sigma_8 = 0.817$, $n_s = 0.96$, $\Omega_m = 0.279$, $\Omega_b = 0.0462$ and $\Omega_\Lambda = 1 - \Omega_m = 0.721$. Each simulation was run with a lean version of the Tree-PM code GADGET-2 (Springel 2005), and followed the dark matter using 1024^3 collisionless particles. One simulation had a box side-length of $L_{\text{box}} = 1200 h^{-1} \text{ Mpc}$ and a particle mass of $m_{\text{part}} = 1.246 \cdot 10^{11} h^{-1} M_\odot$; the other used $L_{\text{box}} = 150 h^{-1} \text{ Mpc}$ and had $m_{\text{part}} = 2.433 \cdot 10^8 h^{-1} M_\odot$. The initial redshifts of the simulations were $z_{\text{in}} = 50$ and $z_{\text{in}} = 70$ for the larger and smaller box, respectively. Using these simulations we are able to probe a wide range of halo masses, spanning $8 \cdot 10^{10} h^{-1} M_\odot < M_h < 10^{14} h^{-1} M_\odot$. These simulations were first studied in Pillepich et al. (2010), and later by Ludlow & Porciani (2011), and we refer the reader to those papers for further details.

Haloos were identified at $z = 0$ using a friends-of-friends (FOF) algorithm (Davis et al. 1986) with a linking length of 0.2 times the mean interparticle distance. Protohaloes were identified by tracing backward to the initial redshift of all subsets of the particles belonging to $z = 0$ FOF haloos. We use the centre of mass of each protohalo as a proxy for its spatial location; the mass-weighted linear velocity provides an estimate of the protohalo's motion. As a test of the sensitivity of our results to the adopted halo finder, we also generated a spherical overdensity (SO) halo catalogue with an overdensity threshold of 200 times the critical density, ρ_c . For a fixed halo mass, the two halo-finders produce results consistent within 10 per cent (in terms of all the bias coefficients) and so, in what follows, we will focus on results obtained for the FOF haloos, and only consider those containing at least 100 particles.

Haloos in each simulation are split into four separate mass bins in order to preserve their peculiar clustering properties. These bins are referred to as 1S to 4S for the small box, and 1L to 4L for the large one. To asses the impact of shot noise in the analysis of our small-box simulation we consider an additional mass bin, labeled bin0S, which includes all haloos with $N \geq 100$. The mass ranges and total number of haloos in each bin are given in Table 1. We note that bins with label ‘S’ refer to masses $M < M_*$ for which

dark-matter haloos are not expected to be in one-to-one correspondence with linear peaks (Ludlow & Porciani 2011).

3.2 Analysis

We construct protohalo density and momentum fields using cloud-in-cell grid assignment on a 512^3 mesh. Velocity fields are obtained by taking the ratio of the momentum and density fields, as described in Scoccimarro (2004). In the case of haloos, these distributions are smoothed to preclude the existence of empty cells; the smoothing scales used are $R_f = 7h^{-1} \text{ Mpc}$ for the large box and $R_f = 1.8h^{-1} \text{ Mpc}$ for the small one. These values are chosen in order to mask the effects of the grid, but we have explicitly verified that our results are not significantly affected by them. All power spectra have been computed using a fast Fourier transform technique.

The discreteness of dark-matter particles and haloos gives rise to a shot-noise component in the spectra. For the density fields, the estimated power spectrum, \hat{P} , includes a shot-noise term which is inversely proportional to the number density of objects \bar{n} (assuming Poisson sampling):

$$\hat{P} = P_{\text{true}} + \frac{1}{\bar{n}}. \quad (19)$$

Shot noise is therefore negligible for the matter spectra but may be significant for that of the haloos. The issue is more severe in Lagrangian space, because fluctuations in the initial conditions are small. We will consider two alternative estimates of the protohalo bias; one is determined from the shot-noise corrected auto-spectrum,

$$b(k) \equiv \sqrt{\frac{P_h(k)}{P(k)}}, \quad (20)$$

and the other from the cross-spectrum,

$$b_{\text{eff}}(k) \equiv \frac{P_{\text{mh}}(k)}{P(k)}. \quad (21)$$

Here the subscript ‘h’ indicates the halo fields, and ‘m’ the matter field (the analogous fields for peaks are indicated with the subscript ‘p’.) The relation between the two is

$$b_{\text{eff}}(k) = b(k) \cdot r(k), \quad (22)$$

where r is the linear correlation coefficient, defined as

$$r(k) = \frac{P_{\text{mh}}(k)}{\sqrt{P(k)P_h(k)}}. \quad (23)$$

These relations tell us that the two definitions of the bias are equivalent *only if* the bias is purely deterministic in Fourier space, i.e. $r = 1$. At leading order, in the model presented by DS, $b_{\text{eff}}(k) = b_\nu + b_\zeta k^2$ and $b(k) = |b_{\text{eff}}(k)|$ (neglecting the filter function). Any stochasticity (represented by the higher order corrections in P_p) will degrade the correlation, yielding different estimates for the bias. Because of this, we will consider both the cross- and auto-spectra to check for a potential stochastic element of the bias.¹

As for the density, we can define two estimates for the

¹ Although the effective first-order bias model by DS is deterministic in Fourier space, it is stochastic in configuration space (Matsubara 1999, Desjacques & Sheth 2010).

velocity bias, that we denote b_θ and $b_{\theta\text{eff}}$, with a correlation coefficient r_θ . There is no conclusive way to subtract the shot noise for the velocity divergence spectrum. Hence we used our simulations to gain some insight into this issue. We introduced an artificial shot noise in the matter spectrum \mathcal{P} by randomly drawing a fraction of the particles and found that $\mathcal{P}_{\text{shot}}(k) \simeq A \cdot k^2$ asymptotically for large k . Therefore we fitted the amplitude factor A to obtain shot-noise corrected power spectra. Note however that other terms could be important at smaller wavenumbers; in this work we only consider data for which $\mathcal{P}_{\text{shot}}(k) < 0.1\hat{\mathcal{P}}$.

The DS model describes the biasing of linear density peaks that are expected to form haloes of a given mass at a specified redshift according to some collapse model (which determines the value for δ_c). However, we analyse the density and velocity fields for the actual FOF and SO protohaloes. These are the quantities of physical interest for studying galaxy clustering in terms of halo occupation models (e.g. Cooray & Sheth 2002). Ludlow & Porciani (2011) showed that the vast majority of haloes in our N-body simulations can be unambiguously associated with linear peaks in the initial conditions when smoothed on the mass scale of the halo. For example, $\gtrsim 70$ per cent of all haloes can be matched with similar-mass peaks in $\delta_S(\mathbf{x})$, and $\gtrsim 90$ per cent for haloes with $M \gtrsim 10^{14} h^{-1} M_\odot$. Note, however, that the correspondence between the DS peaks and protohaloes will not be perfect.² On a given mass scale, some peaks with overdensities at the collapse threshold will evolve into substructures contained within larger virialized haloes (the so-called cloud-in-cloud problem), or to haloes of significantly different mass. On top of this, numerical simulations have shown that the collapse threshold δ_c for haloes of a given mass and redshift has a broad probabilistic distribution rather than a fixed value (Porciani, Dekel & Hoffman 2002; Robertson et al. 2009) and possibly also depends on the form of the adopted smoothing kernel. We consider some of these issues in the following section.

3.3 Barrier heights for top-hat and Gaussian filters

The peak model described in Section 2 requires well-defined spectral moments. However, due to its sharp boundary in real space, the top-hat filter decays very slowly in Fourier space so that the integral defining σ_2^2 is divergent in a LCDM model. Since eqs. (11), (12) and (13) depend on σ_2 , DS instead adopted a Gaussian filter and assumed $\delta_c = \delta_{\text{sc}} = 1.68$. Here, δ_c corresponds to the critical density for the collapse of a spherical top-hat perturbation in an otherwise unperturbed EdS universe, and this does not necessarily apply to peaks in a smoothed Gaussian random field. Another issue is that the validity of the simple spherical collapse model is questionable, at best; the probability of a protohalo or a peak being spherical is null, since it would require the three eigenvalues of the tidal tensor being equal. Sheth, Mo & Tormen (2001) showed that the

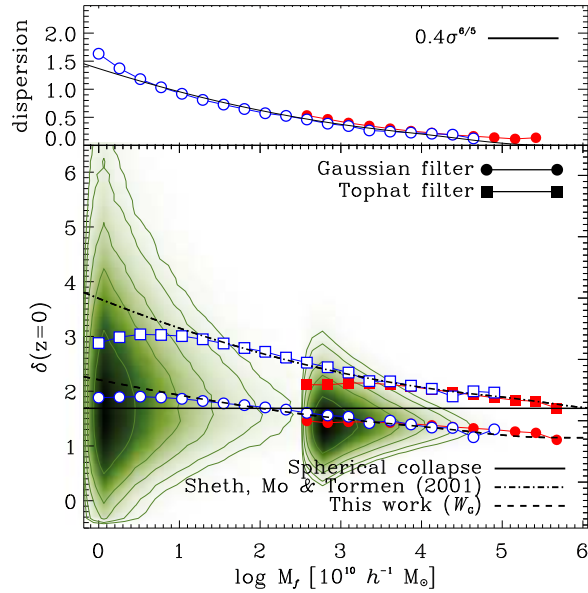


Figure 1. Mass-dependence of the linear overdensities measured at protohalo centres in the initial conditions of our simulations. The shaded regions and contours show the full halo distribution after smoothing with a Gaussian filter; connected circles highlight the median trend. All values of δ_h have been linearly extrapolated to $z = 0$. Open and filled points correspond to our $150 h^{-1}$ Mpc and $1200 h^{-1}$ Mpc boxes, respectively. For comparison, we also show, using boxes, the median trends obtained after smoothing with a top-hat kernel. In both cases, the median trends are well described by eq. (24): the dot-dashed curve shows the SMT result (note that this is not a fit to our simulation data), and the dashed curve shows the result for slightly different values of the free parameters: $\delta_* = 1.15$, $\alpha = 0.37$ and $\beta = 0.515$. The top panel shows the mass dependence of the scatter about the median trend for the Gaussian-filtered case, which is well approximated by a simple power-law, $\Sigma = 0.4 \sigma_0^{6/5}$.

barrier height in the more general ellipsoidal collapse model (Bond & Myers 1996) can be approximated by

$$\delta_{\text{ec}}(M, z_c) = \delta_* \left\{ 1 + \alpha \cdot \left[\frac{\sigma_0^2(R_s(M), z_c)}{\delta_*^2} \right]^\beta \right\}, \quad (24)$$

where $\delta_* = \delta_{\text{sc}}$ is taken from the spherical collapse model, and $\alpha = 0.47$ and $\beta = 0.615$ are determined from fits to the model results. The presence of the dispersion, σ_0 , in eq. (24) results in a mass-dependent barrier height: lower mass haloes require, on average, higher overdensities for collapse since they must hold themselves together against larger tidal forces. It should be emphasized that eq. (24) describes the *mean* barrier height; the scatter about the mean can be approximated by $\Sigma = 0.3 \sigma_0$ (Robertson et al. 2009). These values are valid only for the top-hat filter.

What is the appropriate barrier height corresponding to a Gaussian filter? In Figure 1 we show the linear overdensities measured at protohalo centres of mass after smoothing with a Gaussian filter on the halo mass scale. The shaded regions show the halo data, and connected circles the medians of the distribution. Open points correspond to results from our $150 h^{-1}$ Mpc box simulation, and solid points to our $1200 h^{-1}$ Mpc box run. Squares show the median $\delta_c(M)$ for the same sample of haloes, but after smoothing the lin-

² The measured abundance of haloes in the simulations is of the same order of magnitude as (albeit a bit higher than) the number of peaks with $\nu > 1.68/\sigma_0$ computed as in Bardeen et al. (1986).

ear density field with a top-hat filter instead (note the good agreement with the result of Sheth, Mo & Tormen (2001), shown as a dot-dashed line in Figure 1). All values have been linearly extrapolated to $z = 0$.

It is clear that adopting a Gaussian filter entails lower values of δ_c at all masses³. Nonetheless, our results are still accurately described by eq. (24), albeit with slightly different values for the model parameters: $\delta_* = 1.15$, $\alpha = 0.37$ and $\beta = 0.515$. We show this explicitly in Figure 1 using a dashed line. The one-sigma dispersion about the mean trend is well described by a simple power-law, $\Sigma = 0.4 \sigma_0^{6/5}$, as seen in the upper panel of the plot.

4 RESULTS

In this section we test the predictions of the DS model against the measured density and velocity bias of dark matter protohaloes. In order to do so, we calculate the (model-predicted) bias parameters b_ν , b_ζ and b_σ for each mass bin in both of our simulations. Since the values of b_ν and b_ζ depend on peak height (and hence smoothing scale) we adopt two models for the collapse barrier: one assumes the spherical collapse model (hereafter SG) and the other the ellipsoidal collapse model (hereafter EG). A Gaussian filter is used in both cases. Table 1 lists the bias parameters predicted by the DS model for these choices of collapse barrier.

4.1 Density spectra

In Figure 2 we plot $b(k)$ and $b_{\text{eff}}(k)$ extracted from our simulations,⁴ along with the model prediction (eq. (17)). Although the model is not expected to work for very small scales, we nonetheless show the results for each box up to $k \simeq 1/R_f$ (we remind that R_f is the smoothing scale needed for the velocity field). Overall, the model expression for the initial peak bias is able to describe the simulation results reasonably well. This can be seen from the solid lines in Figure 2, where b_ν and b_ζ have been treated as free parameters and fitted to both the cross- and the auto spectra. However, it is clear that the values for the fit parameters are different in the two cases (see Table 2), implying $b(k) \neq |b_{\text{eff}}(k)|$ or, equivalently, $r(k) \neq 1$. In particular, for the range of masses in Bin 0S, b_{eff} is negative, i.e. $r < 0$. The predictions from the SG and EG barriers, as apparent from the dashed and dotted lines in the right panel in Figure 2, are also negative. Hence the bias model matches more closely b_{eff} rather than b . This is completely expected, because eq. (17) is exact only for the cross-correlation between peaks and matter while it neglects higher-order corrections for the peak autocorrelation. However, neither the SG nor the EG barrier provide the appropriate values for the coefficients. In particular, the EG barrier performs better for low masses (bin 0S), while the situation is reversed for the higher mass bins.

³ At any mass scale, M , the smoothing length of a Gaussian filter exceeds that of a top-hat filter by a factor of $(3\sqrt{\pi/2})^{1/3} \approx 1.55$.

⁴ The values directly measured from the simulations are rescaled by the growth factor $D(z_{\text{in}})$ to match the theoretical estimates, where δ is linearly extrapolated to $z = 0$. Note that the actual Lagrangian bias is a factor $D^{-1} \simeq 40 - 50$ larger than the values reported in the figure.

Figure 2 suggests that the stochasticity is more of a problem for haloes with $M < M_*$, and on smaller scales. Since high-mass haloes are highly correlated with density peaks in the initial conditions (Ludlow & Porciani 2011) and peaks follow eq. (14), the relationship between $\delta_h(\mathbf{k})$ and $\delta(\mathbf{k})$ is likely to be more deterministic for massive haloes. Note, however, that the estimate of r is affected by the shot-noise correction, which is large in our samples. Therefore we cannot draw definitive conclusions regarding stochasticity.

The performance of the model is characterized in another way in Figure 3, where we compare directly the mass dependence of the bias parameters $b_\nu(M)$ and $b_\zeta(M)$ predicted by the SG and EG models to the best-fit values obtained using the parameterization of the cross-spectrum in eq. (17). We do not show the corresponding results from the auto-spectrum because of the uncertain shot-noise subtraction. Figure 3 reveals that overall the b_ν values derived from the SG model are closer to the fitted ones. In contrast, there is almost no difference between the two models for b_ζ . For both parameters the mass dependence follows a different trend when we compare the fits to the models. In particular, the prediction for b_ζ and $M < M_*$ becomes more and more inaccurate with decreasing halo mass (up to a factor of ~ 3 for $M \simeq M_*/15$). On the other hand, in the mass range for which the model was developed ($M > M_*$), b_ζ is overpredicted by a factor of ~ 1.5 , independent of halo mass. Figure 2 shows that the disagreement is even worse when b_ν and b_ζ are obtained from P_h . All of this demonstrates that eqs. (11) and (12) cannot accurately describe the mass dependence of the Lagrangian density bias, especially for $M < M_*$. We will discuss possible reasons for this in Section 5, but first turn our attention to the velocity spectra.

4.2 Velocity spectra

Figure 4 shows $b_\theta(k)$ and $b_{\theta\text{eff}}(k)$ for bins 1S-4S and 1L-4L; the theoretical model, $b_{\text{vel}}(k)$, is also plotted. The data have been “de-smoothed”, i.e. they have been divided by a filter function with smoothing scale R_f , the same used to smooth the velocity field in the first place. It is apparent that on large scales the two estimates of the bias coincide, i.e. $r_\theta \simeq 1$, indicating a strong correlation between the fields. Overall, we can conclude that the velocity bias is deterministic to a good approximation.

There is an excellent agreement (better than 10 per cent) between the simulation results and the model predictions for all mass bins at scales $k < 0.1 \ h \text{Mpc}^{-1}$ for the large box and $k < 0.3 \ h \text{Mpc}^{-1}$ for the small one. Therefore, the peak model provides a faithful description of the velocity bias.

5 SUMMARY

We have investigated the Lagrangian bias of dark-matter haloes by testing the theoretical model proposed by DS against N-body simulations of structure formation. The model assumes that haloes form from density peaks and predicts a scale-dependent bias for both the density and velocity fields. Our main results can be summarized as follows.

- When averaged over a spherical Lagrangian volume

Bin	Mass range	# haloes	\bar{M}	b_ν		b_ζ		b_σ	R_s
	$(10^{12} h^{-1} M_\odot)$		$(10^{12} h^{-1} M_\odot)$			$(h^{-2} \text{ Mpc}^2)$		$(h^{-2} \text{ Mpc}^2)$	$(h^{-1} \text{ Mpc})$
				SG	EG	SG	EG		
0S	0.08 – 0.8	106746	0.2986	-0.31	-0.23	0.63	0.61	0.92	0.62
1S	0.08 – 0.1	21990	0.08961	-0.30	-0.21	0.26	0.25	0.45	0.42
2S	0.1 – 0.15	30610	0.1235	-0.30	-0.22	0.33	0.32	0.55	0.46
3S	0.15 – 0.3	32322	0.2165	-0.31	-0.23	0.49	0.48	0.76	0.56
4S	0.3 – 0.8	21824	0.4934	-0.31	-0.24	0.92	0.90	1.24	0.74
1L	12.46 – 16	146839	14.15	0.05	-0.08	11.3	11.5	8.75	2.26
2L	16 – 25	182006	20.25	0.18	-0.003	14.7	15.2	10.8	2.54
3L	25 – 40	121146	32.05	0.40	0.12	20.5	21.5	14.0	2.96
4L	40 – 100	114367	65.99	0.92	0.44	34.5	37.1	21.2	3.77

Table 1. Mass range, number of haloes, average mass and bias parameters (both weighted by halo counts) for the nine different mass bins used in our study. The first five belong to the small-box simulation; the last four to the large-box simulation. The bias parameters are computed according to the two models for the peak height described in the text: the spherical and ellipsoidal collapse models. All values have been obtained adopting a Gaussian filter.

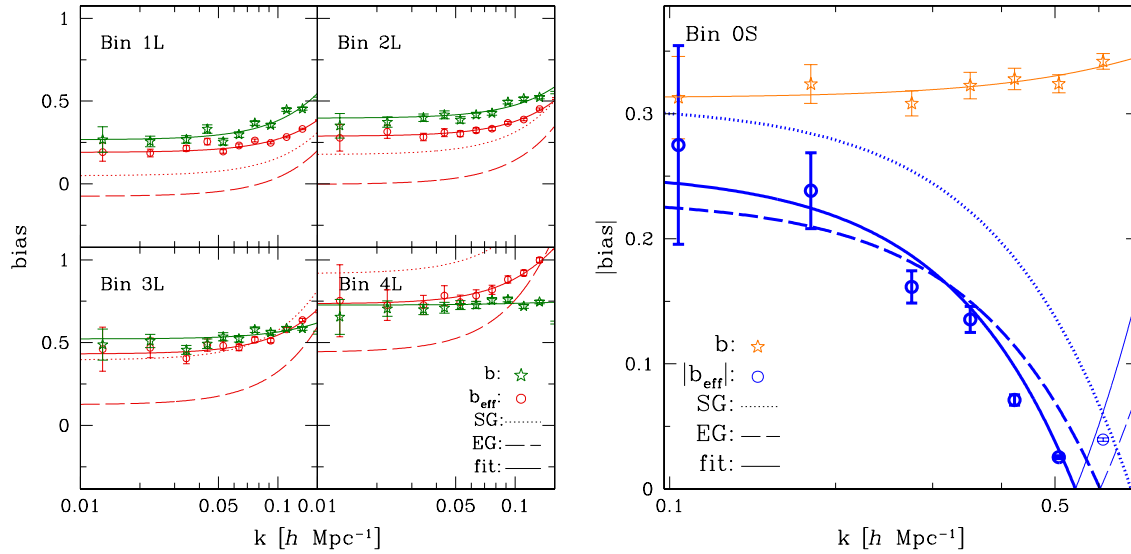


Figure 2. *Left:* Stars and open circles plot, respectively, $b(k)$ and $b_{\text{eff}}(k)$ for the four separate mass bins in our large simulation box. Dotted lines show the predictions obtained for the spherical collapse model, and dashed lines those of the ellipsoidal collapse model adopting a Gaussian filter. Solid lines are the best-fits to the data points. *Right:* Stars and open circles correspond to $b(k)$ and $|b_{\text{eff}}(k)|$, respectively. As in the left panels, dotted and dashed line show to the SG and EG models, and solid lines are the best-fits to the data. Thick lines indicate negative values of the bias. In all cases, errors are propagated assuming that the uncertainty in the power-spectrum is $\sigma(k) = \sqrt{2/N(k)} \cdot P(k)$, where $N(k)$ is the number of modes in each k bin.

Bin	b_ν				$b_\zeta (h^{-2} \text{ Mpc}^2)$			
	P_{mh}		P_{h}		P_{mh}		P_{h}	
	FOF	SO	FOF	SO	FOF	SO	FOF	SO
0S	-0.25	-0.24	-0.31	-0.30	0.86	0.81	0.14	0.11
1L	0.19	0.22	0.27	0.37	8.8	7.9	12.6	12.0
2L	0.29	0.31	0.40	0.39	10.3	9.3	9.5	8.8
3L	0.43	0.47	0.52	0.54	13.9	13.1	6.7	5.9
4L	0.73	0.75	0.73	0.73	21.8	20.9	6.4	5.4

Table 2. Best-fit values for the density bias parameters from the cross-spectra and the auto-spectra. Uncertainties are always at the few per cent level. Haloes are identified either with the FOF or the SO algorithms.

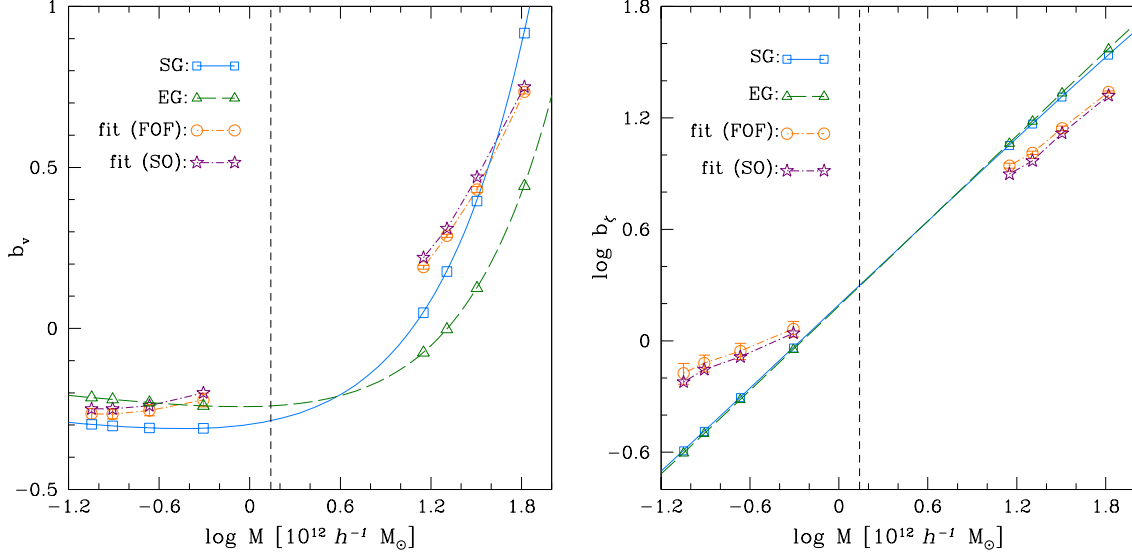


Figure 3. Density bias parameters, b_v (left) and b_ζ (right), plotted as a function of halo mass. Orange circles with error bars correspond to the best-fit values obtained from the cross-spectra of haloes identified with the FOF algorithm. The corresponding values for SO haloes are shown with purple stars. The solid and dashed lines show, respectively, the predictions of the DS model for the spherical collapse model, and for the ellipsoidal model with a Gaussian filter. The vertical dashed black lines mark M_* .

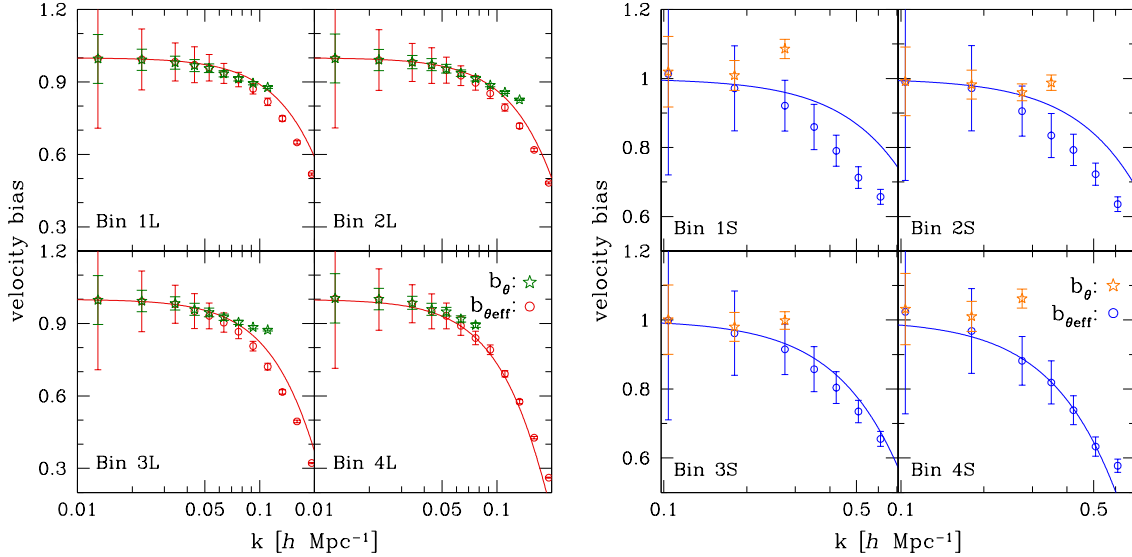


Figure 4. Stars and circles show $b_\theta(k)$ and $b_{\theta\text{eff}}(k)$, respectively, for haloes in our large (left) and small (right) simulation boxes. The solid line is the DS model prediction (eq. (15) with R_s given in Table 1), which is independent of peak height. Errors are propagated as in Fig. 2. Note that we only show $b_\theta(k)$ on scales over which the shot-noise is sub-dominant, as stated in Section 3.2.

containing the appropriate mass, the linear density contrast measured at protohalo centres depends sensitively on the choice of smoothing kernel. For a Gaussian kernel, for example, the resulting density contrasts are systematically lower than those computed using a top-hat filter. This is because, at fixed mass, the smoothing length of a Gaussian kernel exceeds that of a top-hat filter by a factor of about 1.55 resulting in systematically lower density estimates. Nonetheless, the median barrier height computed with a Gaussian kernel can be accurately parameterized by the same fitting formula first advocated by Sheth, Mo & Tormen (2001) for

the case of a top-hat filter, albeit with different values for the numerical parameters. We use this result to approximate the collapse threshold for dark matter halo formation when adopting a Gaussian filter.

- The functional forms for the density and velocity bias relations derived by DS - our eqs. (17) and (18) - accurately describe the results obtained from our simulations, provided the parameters of the model are allowed to vary with respect to the model-predicted values. In both cases, the Lagrangian bias is characterized by a constant term that dominates on

very large scales, and a scale-dependent term proportional to k^2 .

- Quantitatively, the velocity bias predicted by the DS model is able to reproduce the measured protohalo velocity bias in our simulations to better than 10 per cent, provided we limit ourselves to quasi-linear scales ($k \leq 0.3 \, h \, \text{Mpc}^{-1}$). The predicted density bias (eqs. (11) and (12)), on the other hand, does not match the Lagrangian density bias extracted from the simulations. This is likely due to the more complex nature of the density bias, which depends additionally on peak height and on the exact definition of a protohalo. These results are independent of whether one adopts a barrier height consistent with either the spherical or ellipsoidal collapse model.

- We have measured the mass dependence of the density bias, b_ν and b_ζ , by fitting the density power-spectra obtained for haloes in several different mass bins in each of our two simulations. The most massive haloes identified in our simulations are the most strongly biased, and have characteristic overdensities that correlate with the underlying matter density. In contrast, the distribution for low mass haloes ($M_h < 10^{12} h^{-1} M_\odot$) exhibits an anti-correlation. A similar trend is also predicted by the DS model, although with noticeable differences (see Figure 3). We emphasize that the best-fit values for b_ν and b_ζ obtained in our analysis apply for a Λ CDM cosmogony (with our adopted cosmological parameters) and only over the limited mass range probed by our simulations. Future work should consider how the Lagrangian density bias depends on the underlying cosmology.

- Our comparison of the auto- and cross-spectra in Section 4 suggests the presence of a stochasticity in the Fourier-space density bias of dark matter protohaloes, but none for the velocity bias. This is in disagreement with the DS model for the bias at leading order, and seems to corroborate the need for higher-order terms in the expression for the auto-spectrum of the protohaloes, as predicted in Desjacques et al. (2010). However, we cannot draw firm conclusions regarding stochasticity in the bias estimates due to uncertainties in the shot-noise subtraction.

We have tested the Lagrangian bias model of DS against a pair of high resolution N-body simulations of structure formation and found that it is able to accurately reproduce the velocity bias, but not that of the density. Our analysis focused on protohaloes, the high redshift progenitors of $z = 0$ dark-matter haloes, whereas the model describes the biasing of density peaks. One possible explanation for the differences in the model predictions and simulation results comes from the differences between the expressions for the bias parameters: b_ν , b_ζ and b_σ . The latter of the three is solely determined by the linear matter power spectrum and the smoothing scale corresponding to a given mass, M . The density bias parameters, however, depend additionally on explicit properties of the peaks, such as their height, ν , mean curvature, \bar{u} , and on an assumed collapse threshold for their identification as haloes of a given mass. Figure 1 shows that there is a large halo-to-halo variation in ν at any given mass scale; characterizing the collapse threshold as a single mass-dependent value may, therefore, be too simplistic. This added complexity introduces a significant margin for error in the model's estimates of the density bias. It remains to be seen whether more realistic models of the collapse bar-

rier - such as those that account for the statistical scatter in the linear over-densities of protohaloes at a given mass - will improve the model's predictive power.

Another possibility for the discrepancies stems from the fact that we are identifying linear density peaks with protohaloes in our simulation initial conditions. Although the majority of our dark matter protohaloes form in the vicinity of linear density peaks of the same characteristic mass, the fate of *all* peaks with the same mass and overdensity is unclear. Uncertainties associated with the identification of protohaloes within the linear density field may have adverse effects on the predictive power of the density bias model. A more detailed understanding of how protohaloes map onto linear density peaks, and vice versa, will, no doubt, provide valuable insight into the mechanisms behind halo biasing.

ACKNOWLEDGMENTS

AE acknowledges financial support from the SFB-Transregio 33 “The Dark Universe” by the Deutsche Forschungsgemeinschaft (DFG) and a scholarship from the Bonn-Cologne Graduate School (BCGS). We acknowledge interesting discussion on halo finders with Steffen Knollmann and Andrea Macciò. We would like to thank Jeremy Tinker for providing us with his SO halo finder, and for help applying it to our simulations. We are very grateful to the referee, Vincent Desjacques, for useful suggestions and valuable insights.

REFERENCES

- Bardeen J.M., Bond J.R., Kaiser N., Szalay A.S., 1986, ApJ, 304, 15
- Bond J.R., Cole S., Efstathiou G., Kaiser N., 1991, ApJ, 379, 440
- Bond J.R., Myers S.T., 1996, ApJ Suppl., 103, 1
- Catelan P., Lucchin F., Matarrese S., Porciani C., 1998, MNRAS, 297, 692
- Catelan P., Porciani C., Kamionkowski M., 2000, MNRAS, 318, L39
- Cole S., Kaiser N., 1989, MNRAS, 237, 1127
- Cooray A., Sheth R.K., 2002, PhR, 372, 1
- Davis M., Efstathiou G., Frenk C. S., White S. D. M., 1985, ApJ, 292, 371
- Desjacques V., 2008, Phys. Rev. D, 78, 103503
- Desjacques V., Sheth R.K., 2010, Phys. Rev. D, 81, 023526
- Desjacques V., Crocce M., Scoccimarro R., Sheth R.K., 2010, Phys. Rev. D, 82, 103529
- Elia A., Kulkarni S., Porciani C., Pietroni M., Matarrese S., 2011, MNRAS, 416, 1703
- Frenk C. S., White S. D. M., Davis M., Efstathiou G., 1988, ApJ, 327, 507
- Fry J.N., Gaztañaga E., 1993, ApJ, 413, 447
- Kaiser N., 1984, ApJ, 284, L9
- Komatsu E., 2009, ApJ Suppl., 180, 330
- Gao L., White S.D.M., Jenkins A., Frenk C.S., Springel V., 2005, MNRAS, 363, 379
- Giannantonio T., Porciani C., 2010, Phys. Rev. D, 81, 063530
- Hoffman Y., Shaham J., 1985, ApJ, 297, 16
- Jing Y.P., 1998, ApJ, 503, L9

- Jing Y.P., 1999, *ApJ*, 515, L45
 Ludlow A., Porciani C., 2011, *MNRAS*, 413, 1916
 Matsubara T., 1999, *ApJ*, 525, 543
 Matsubara T., 2011, *Phys. Rev. D*, 83, 083518
 Mo H.J., White S.D.M., 1996, *MNRAS*, 282, 347
 Mo H.J., Jing Y.P., White S.D.M., 1997, *MNRAS*, 284, 189
 Peacock J.A., Heavens A.F., 1985, *MNRAS*, 217, 805
 Pillepich A., Porciani C., Hahn O., 2010, *MNRAS*, 402, 191
 Pollack J.E., Smith R.E., Porciani C., 2011, *arXiv* 1109.3458
 Porciani C., Catelan P., Lacey C., 1999, *ApJ*, 513, L99
 Porciani C., Dekel A., Hoffman Y., 2002, *MNRAS*, 332, 339
 Porciani C., Matarrese S., Lacey C., Lucchin F., Catelan P., 1998, *MNRAS*, 298, 109
 Press W. H., Schechter P., 1974, *ApJ*, 187, 425
 Robertson B.E., Kravtsov A.V., Tinker J., Zentner A.R., 2009, *ApJ*, 696, 636
 Roth N., Porciani C., 2011, *MNRAS*, 415, 829
 Scannapieco E., Barkana R., 2002, *ApJ*, 571, 585
 Scannapieco E., Thacker R.J., 2005, *ApJ*, 619, 1
 Scoccimarro R., 2004, *Phys. Rev. D*, 70, 083007
 Seljak U., Warren M.S., 2004, *MNRAS*, 355, 129
 Sheth R.K., Tormen G., 1999, *MNRAS*, 308, 119
 Sheth R.K., Mo H.J. & Tormen G., 2001, *MNRAS*, 323, 1
 Springel V., 2005, *MNRAS*, 364, 1105
 Tinker J.L., Weinberg D.H., Zheng Z., Zehavi I., 2005, *ApJ*, 631, 41
 Tinker J., Robertson B.E., Kravtsov A.V., Klypin A., Warren M.S., Yepes G., Gottlöber S., 2010, *ApJ*, 724, 878
 Zel'dovich Ya.B., 1970, *A & A*, 5, 84